IMPACT VAPORIZATION CRITERIA DURING PLANET FORMATION. E. J. Davies[1], S. Root[2], P. J. Carter[1], M. S. Duncan[1], D. K. Spaulding[1], R. G. Kraus[3], S. T. Stewart[1], S. B. Jacobsen[4]. [1]Department of Earth and Planetary Sciences, U. California, Davis, CA (ejdavies@ucdavis.edu), [2]Sandia National Laboratories, [3]Lawrence Livermore National Laboratory, [4]Department of Earth and Planetary Science, Harvard University.

Introduction: Collisions are an important process during planet formation. Collision outcomes are diverse and complex, ranging from the growth of planetesimals to moon-forming giant impacts [1, 2]. Because collisions deposit energy and redistribute material during planet formation, they can alter the thermal and geochemical evolution of growing planets [3-6]. During an impact, chemical evolution is driven by melting and vaporization from the irreversible work deposited by shock compression followed by adiabatic decompression to ambient conditions. The impact criteria to reach the onset of vaporization depends on the equations of state of the constituent materials. Here, we review and recalculate vaporization criteria for major planetary minerals: water ice, quartz, forsterite, and iron.

We use the entropy method to calculate phase changes after shock compression and isentropic decompression [7]. See [8] for a schematic of the thermodynamic path of a parcel of material during an energetic impact that illustrates the entropy method. In a shock, the pressure, temperature, and entropy increase to a state defined by the material's shock Hugoniot. The shocked material decompresses via a sound wave. Therefore, the thermodynamic path of decompression is isentropic for a single phase, and the entropy of the decompressed state is equal to the entropy of the shocked state. The decompressed phase is determined by this entropy and the ambient pressure of the surroundings. When the final entropy falls in the boundary between two phases (e.g., liquid and vapor), the lever rule is used to determine the mass fraction of each phase.

Previous estimates of shock-induced melting and vaporization typically reported the criteria for phase changes upon decompression to Earth's atmospheric pressure at 10^5 Pa (1 bar) for material starting at STP. However, during accretion, the pressure of the protoplanetary disk is more appropriate: 1 to 10 Pa at 1 AU [9]. These pressures are close to the triple points of silicates and iron. The onset of vaporization is also influenced by the initial temperature, which may be much warmer in the interiors of differentiating bodies.

Methods and Results: The vaporization criteria for water ice was derived using the entropy on the shock Hugoniot from the 5-phase equation of state table, developed in [10] and experimentally validated in [11]. Shock-induced vaporization criteria for 100 K and 263 K water ice are tabulated in [11]. We used the vapor curves from [12, 13]. The vaporization criteria for porous water ice was based on the beginning of the liquid region on the Hugoniot derived from [14]. Additional porous ice vaporization criteria, derived from the 5-phase equation of state table, are available in [15]. For a release pressure of 1 Pa, the onset of vaporization of 150 K ice is ~1 km s^{-1} for solid ice and ~1.5 km s^{-1} for porous ice for symmetric planar impact conditions.

The vaporization criteria for quartz (SiO_2) are based on the experiments and absolute entropy calculations in [16]. We used the revised M-ANEOS vapor curve from [16]. This is a conservative value for the onset of vaporization upon release to the triple point because we have neglected the enthalpy of melting cristobalite, which leads to a reduction in entropy of about 74 J/K/kg [17] for the onset of sublimation. The triple point pressure of about 2.6 Pa for SiO_2 was determined by [18]. The fitted equation for entropy on the α-quartz Hugoniot from [16] (Eq. 7) was valid from 110 to 800 GPa. Here, we extend the fit to lower pressures, into the solid region along the Hugoniot using the stishovite equation of state model in [16]. In deriving the associated impact velocities, we used the Hugoniot from [19].

Heating quartz above 500 K reduces the critical pressure for vaporization to values below the pressures where the entropy in the shock is experimentally constrained. We used the entropy for quartz at 10^5 Pa and 500 K from [20] and shifted the entropy on the room-temperature Hugoniot to estimate the 500 K value. Quartz at temperatures near the solidus of differentiated planetesimals will vaporize upon shock and release after very modest impact velocities, well below 4 km s^{-1}.

The vaporization criteria for forsterite (Mg_2SiO_4) are based on the experiments from [21] and absolute entropy calculations from [22]. The triple point pressure of 5.2 Pa for forsterite was experimentally determined by [23]. We used the vapor curve from the M-ANEOS model, developed in [24], neglecting the enthalpy of fusion at the triple point.

The vaporization criteria for 1200 K forsterite was estimated using the heat capacity from [25]. The entropy and temperature on the experimentally-constrained Hugoniot were shifted to estimate the vaporization criteria. For warm forsterite (1200 K), the onset of vaporization is ~6 km s^{-1}.

The vaporization criteria for iron (Fe) are based on the experiments and absolute entropy calculations from [26]. The triple point pressure of 3 Pa for iron is from the vapor curves in [27]. The entropy of vaporization at 10^5 Pa is taken from [20]. The entropy of vaporization at the triple point is estimated using the entropy of δ-iron at the melting point at 10^5 Pa from [20]. The entropy on the iron Hugoniot presented in supplementary Eq. 11 in [26] was valid from 300 to 1000 GPa. We used the Hugoniot for iron beginning at 1500 K and 1 GPa from [26] supplementary Eq. 11 to derive the estimate for incipient vaporization of a warm iron core. For warm iron (1500 K), the onset of vaporization is ~5.4 km s^{-1}.

Figure 1 shows the required orbital eccentricities of mean relative velocities to meet the critical velocities derived above, defined by $V_{rel} \sim eV_{kep}$, where e is the orbital eccentricity of a population of bodies and V_{kep} is the circular Keplerian velocity at each semi-major axis. Based on N-body simulations of planet formation, the required impact velocities are readily achieved near growing planets, in resonance with the giant planets, and during migration of the giant planets [28].

Figure 2 shows that an impact that creates a small vapor fraction increases the volume of the system by orders of magnitude. Nearly all impact generated vapor plumes are quickly expanding structures that reach large volumes. See [8, 29] for discussion of the thermodynamics of impact vapor plumes.

Conclusions: Low ambient pressures in the nebula and high initial temperatures significantly reduce the critical impact velocities needed for the onset of vaporization. Impact-induced vaporization was a significant process during planet formation [28].

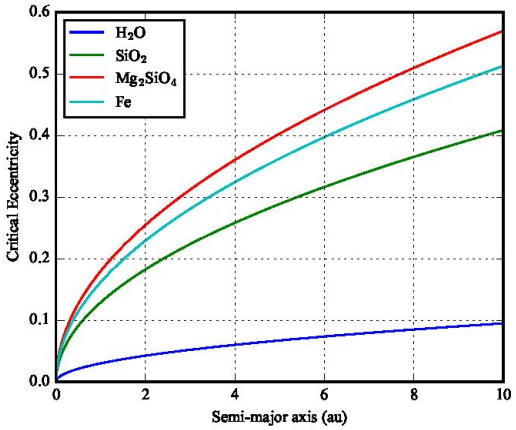

Fig. 1: Critical eccentricities corresponding to relative velocities that induce impact vaporization versus semi-major axis. Critical velocities correspond to 150 K ice and 1200 K forsterite, 1500 K iron and 500 K silica. In the inner solar system, the critical eccentricities are attained in many planet formation scenarios [28].

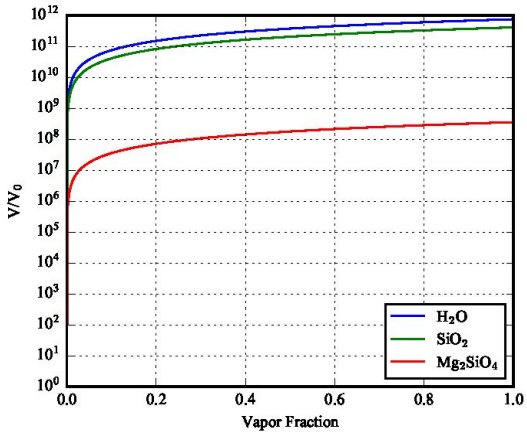

Fig. 2: Decompressed volume normalized to the pre-shocked volume vs. shock-induced vapor fraction. The change in volume upon decompression to ambient pressures (1-10 Pa) is orders of magnitude larger than the initial state, even for very small vapor fractions.

Acknowledgments: Sandia National Laboratories is a multimission laboratory managed and operated by National Technology & Engineering Solutions of Sandia, LLC, a wholly owned subsidiary of Honeywell International Inc., for the U.S. Department of Energy's National Nuclear Security Administration under contract DE-NA0003525. Prepared by LLNL under Contract DE-AC52-07NA27344.

References: [1] Leinhardt Z. M. & Stewart S. T. (2012) *ApJ* ***745***, 79. [2] Lock S. J. & Stewart S. T. (2017) *JGR: Planets* **122.5**: 950-982. [3] Stewart S. T. & Leinhardt Z. M. (2012) *ApJ* **751.1**: 32. [4] Asphaug E. (2010) *CEG* **70.3**: 199-219. [5] Carter P. J. et al. (2015), *ApJ* **813**, 72. [6] Carter P. J. et al. (2018), *EPSL* **484**, 276-286. [7] Ahrens T. & O'Keefe J. D. (1972) *The Moon* **4.1-2**: 214-249. [8] Davies E. J. et al. (2019) *LPSC* ***50***, abs1:1256. [9] Wood J. A. (2000) *FDTP*: 87-93. [10] Senft L. E. & Stewart S. T. (2008) *MPS* **43.12**: 1993-2013. [11] Stewart S. T. et al. (2008) *GRL* **35.23**. [12] Wagner W. & Pruß A. (2002) *JPCRD* **31.2**: 387-535. [13] Feistel R. & Wagner W. (2007) *GCA* **71.1**: 36-45. [14] Stewart S. T. & Ahrens T. (2004) *AIP* **706.1**: 1478-1483. [15] Kraus R. G. et al. (2011) *Icarus* **214.2**: 724-738. [16] Kraus R. G. et al. (2012) *JGR: Planets* **117:** E9. [17] Richet P. et al. (1982) *GCA* **46.12**: 2639-2658. [18] Mysen B. O. & Kushiro I, (1988) *AM* **73**, no. 1-2: 1-19. [19] Knudson M. D. & Desjarlais M. P. (2009) *PRL* **103.22**: 225501. [20] Chase M. W. & Davies C. (1985) *JPCRD* **14**: 1856. [21] Root S. et al. (2018) *GRL* **45.9**: 3865-3872. [22] Davies E. J. et al. (2019) in prep. [23] Nagahara H. et al. (1994) *GCA* **58.8**: 1951-1963. [24] Melosh H. J. (2007) *MPS* **42.12**: 2079-2098. [25] Gillet P. et al. (1991) *JGR: Solid Earth* **96.B7**: 11805-11816. [26] Kraus R. G. et al. (2015) *Nature Geoscience* **8.4**: 269. [27] Alcock C. et al (1984) *CMQ* **23**: 309-313. [28] Carter P. J. et al. (2019) *LPSC* ***50***, abs1:1246. [29] Stewart S. T. et al. (2019) *LPSC* ***50***, abs1:1250.